

Article

A New Approach for Production Prediction in Onshore and Offshore Tight Oil Reservoir

Kaixuan Qiu ^{1,2}, Kaifeng Fan ³, Xiaolin Chen ⁴, Gang Lei ^{5,6,*} , Shiming Wei ^{7,*}, Rahul Navik ¹ and Jia Li ^{4,*} 

- ¹ Jiangmen Laboratory of Carbon Science and Technology, Jiangmen 529100, China; qiukx940908@163.com (K.Q.); rahulnavik@hkustgz-jcl.ac.cn (R.N.)
² The University of Hongkong, Hongkong 999077, China
³ College of Oceanography, Hohai University, Nanjing 210098, China; 18871388135@163.com
⁴ Society Hub, The Hong Kong University of Science and Technology (Guangzhou), Nansha, Guangzhou 511400, China; hljchan334@connect.hkust-gz.edu.cn
⁵ Faculty of Engineering, China University of Geosciences (Wuhan), Wuhan 430074, China
⁶ Shenzhen Research Institute, China University of Geosciences, Shenzhen 518063, China
⁷ College of Science, China University of Petroleum (Beijing), Beijing 102249, China
* Correspondence: leigang@cug.edu.cn (G.L.); we_shiming@163.com (S.W.); leeja@ust.hk (J.L.)

Abstract: Rapid technological advances have accelerated offshore and onshore tight oil extraction to meet growing energy demand. Reliable tools to carry out production prediction are essential for development of unconventional reservoirs. The existed tri-linear analytical solutions are verified to be versatile enough to capture fundamental flow mechanisms and make accurate production predictions. However, these solutions are obtained in Laplace space with the Laplace transform and numerical inversion, which may lead to uncertainty in the solution. In this paper, a general analytical solution is derived in real-time space through integral transform and average pressure substitution. Namely, the partial differential equations describing subsurface fluid flow are firstly triple-integrated and then the obtained volume average pressure are replaced with the rate-dependent expressions. Furthermore, the ordinary differential equations related to oil rate are solved analytically in real-time space. To validate our model, this derived solution is verified against two numerical models constructed with two typical physical configurations. The great match indicates the accuracy and applicability of the analytical solution. According to the developed workflow, two field cases including offshore and onshore tight oilfield data are selected for history matching and production prediction. This new approach not only makes the obtained solution more simplified, but also helps field engineers diagnose flow patterns more quickly to better optimize production schemes.

Keywords: tri-linear flow; offshore tight oilfield; analytical solution; history matching; production prediction



Citation: Qiu, K.; Fan, K.; Chen, X.; Lei, G.; Wei, S.; Navik, R.; Li, J. A New Approach for Production Prediction in Onshore and Offshore Tight Oil Reservoir. *J. Mar. Sci. Eng.* **2023**, *11*, 2079. <https://doi.org/10.3390/jmse11112079>

Academic Editor: Timothy S. Collett

Received: 22 September 2023

Revised: 20 October 2023

Accepted: 25 October 2023

Published: 30 October 2023



Copyright: © 2023 by the authors. Licensee MDPI, Basel, Switzerland. This article is an open access article distributed under the terms and conditions of the Creative Commons Attribution (CC BY) license (<https://creativecommons.org/licenses/by/4.0/>).

1. Introduction

The global demand for oil/gas is increasing sharply over the past few decades [1]. Unconventional resources have attracted domestic and international attention due to its abundance in onshore and offshore oilfields, particularly for tight oil with matrix permeability less than 0.1 mD. [2]. According to the statistical results from the Energy Information Administration (EIA), the contribution from offshore oilfields has reached nearly 30% of global production [3]. Well performance is considered as a critical factor because of its close relationship with economics of unconventional reservoirs. Therefore, advanced techniques for unconventional reservoirs are constantly updated to generate the accurate production prediction tools by covering the relative petrophysical properties of subsurface fluid storage and flow [4–7].

Unconventional reservoirs, unlike conventional reservoirs, must be hydraulically fractured prior to commercial production of hydrocarbons. The highly conductive fracture

networks are created for subsurface fluid to flow from the tight matrix to the wellbore. The widely used techniques for flow pattern analysis and production prediction in these reservoirs include numerical simulation and analytical models [8–12]. Certainly, numerical simulation methods have good flexibility and can also deal with various complicated reservoir seepage problems. However, there will be a time-consuming and computationally inefficient process when they are adopted to compute the complex fracture geometry with a large number of grids [13,14]. Generally speaking, the analytical model offers relative simplicity and it can cover the fundamental flow mechanism with simple solutions. A large number of analytical models have been proposed to study the matrix–fracture communication and well performance in unconventional reservoirs. El-Banbi [15] observed the long-term half-slope line on a log–log plot of oil rate against production time and derived a series of analytical solutions to analyze the transient linear behavior in tight oil reservoirs. On the basis of El-Banbi’s model, Bello [16] applied the transient-linear-flow model in fractured shale reservoirs and developed many asymptotic analysis equations to describe observable linear flow regimes. For most cases of unconventional oil/gas reservoir development, the communication between the tight matrix and complex fractures is thought of as the transient linear flow in the stimulated reservoir volumes (SRV). Brown et al. [17] presented a general tri-linear flow model describing the sequential flow among the hydraulic fracture region, the stimulated region with complex fracture networks and the low-permeability matrix region beyond hydraulic fractures. Moreover, Stalgorova and Matter [18] provided another tri-linear flow analytical model with a different configuration to consider complex branch fractures. The surrounding low-permeability matrix regions in their model are parallel to the hydraulic fractures. One of the key advantages of the trilinear flow model is that it is sufficient to study the key characteristics of flow convergence toward a fractured horizontal well within the stimulated reservoir volume. Because the completion process associated with multifracture horizontal wells can often significantly alter rock stresses and induce natural fractures, it is important that the complex interplay of flow among matrix, natural fractures and hydraulic-fractures can be captured in pressure-transient models. More importantly, the two model configurations are both typical and have been validated to accurately predict production in unconventional reservoirs.

In this paper, we present a new approach based on integral transform and average pressure substitution to directly derive an analytical solution in real-time space [19–21]. Firstly, the fractured formation is divided into three regions based on the two typical tri-linear conceptual models. Then, the sequential transient linear flow among three regions can be expressed by partial differential equations (PDEs). Furthermore, the PDEs are firstly transformed into ordinary differential equations (ODEs) and then solved analytically in real-time space through integral transform and average pressure substitution rather than Laplace transform and numerical inversion [22]. Finally, the analytical solution is verified with two classical equivalent numerical models and applied to two field cases from the onshore and offshore oilfield for production prediction.

2. Theory and Model Development

Commercial production from unconventional oil reservoirs (ultra-low permeability) depends on advanced horizontal well techniques with multistage hydraulic fracturing. Because of uncertain fracture branching, some stimulated regions are created around hydraulic fractures, which are often defined and modeled as regions of high permeability. Therefore, it is vital to choose appropriate conceptual models for simulating fluid flow. Two typical tri-linear conceptual models presented, respectively, by Brown et al. [17] and Stalgorova and Matter [18] are adopted in this paper. The whole analytical models are constructed on basis of these two models. Figure 1a,b are both the schematic of the reservoir with a multi-stage fractured horizontal well. There are three regions including a hydraulic fracture region that is individually connected to the well, a stimulated region (gray color) with higher permeability around each hydraulic fracture and an un-stimulated region (white color) with lower permeability connected to the stimulated region. The difference

of the two model is the connection between the un-stimulated region and the stimulated region. It means that different reservoir configurations are also considered in the work. Figure 1c,d present the plan view, which is an idealized representation of the trilinear-flow model used to develop fluid flow equations. The blank arrows represent the flow direction. For the two conceptual models, the systems are assumed to be symmetrical, and no-flow boundaries exist in the symmetry plane between fractures as a result of the interference of flow. Therefore, one quarter of the reservoir (contained in a red dashed box) is adopted to construct the analytical model.

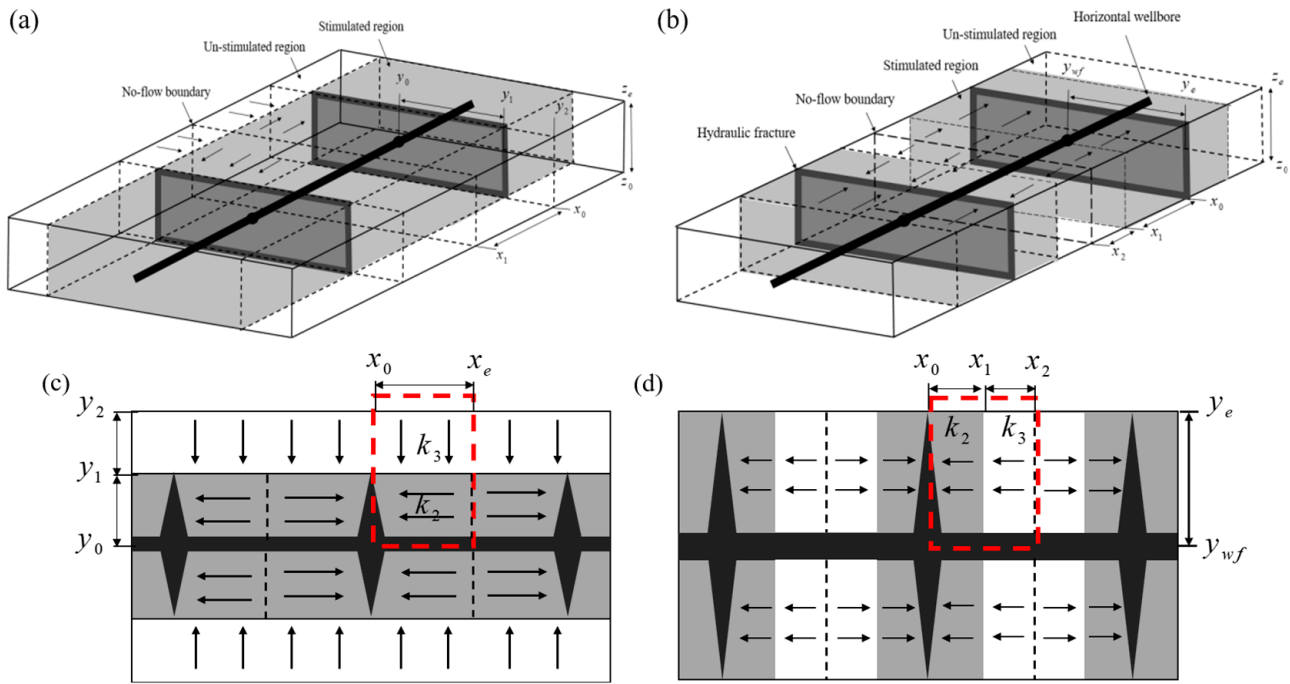


Figure 1. Schematic of a multi-stage fractured horizontal well based on two conceptual models. (a,b) 3D schematic. (c,d) Plan view.

Prior to develop the mathematical model, the model assumptions must be defined to simplify the derivation. The specific assumptions are as follows:

1. The reservoir is homogeneous, thick uniformly and isothermal.
2. Fluid flow is single phase and 1D linear in each region.
3. The whole production process is under constant bottom-hole pressure.
4. The entire flow system follows symmetry and continuity.
5. The effect of gravity and capillary forces are neglected.

Model 1: Based on Brown’s conceptual model

Based on the above model assumptions, the mathematical models can be constructed through describing the transient linear flow process in different regions. Firstly, the governing equation for fluid flow in an un-stimulated region defined as Region 3 can be expressed as

$$\frac{\partial^2 p_{B3}}{\partial x^2} + \frac{\partial^2 p_{B3}}{\partial y^2} + \frac{\partial^2 p_{B3}}{\partial z^2} = \frac{(\phi\mu c_t)_{B3}}{k_{B3}} \frac{\partial p_{B3}}{t} \tag{1}$$

The pressure in Region 3 is considered to be the initial reservoir pressure before fluid flow occurs.

$$p_{B3}(x, y, z, 0) = p_i \tag{2}$$

The outer boundary of the Region 3 is assumed to be a no-flow boundary. Therefore, the appropriate mathematical expression for the outer boundary condition is given by

$$\left. \frac{\partial p_{B3}}{\partial x} \right|_{x=x_0} = 0 \tag{3}$$

$$\left. \frac{\partial p_{B3}}{\partial y} \right|_{y=y_2} = 0 \tag{4}$$

$$\left. \frac{\partial p_{B3}}{\partial z} \right|_{z=z_0, z_e} = 0 \tag{5}$$

Because of the symmetry, there is no fluid flow occurs at $x = x_e$.

$$\left. \frac{\partial p_{B3}}{\partial x} \right|_{x=x_e} = 0 \tag{6}$$

Based on the assumption of continuity, the inner boundary condition can be expressed as

$$\frac{k_{B3}}{\mu} \left. \frac{\partial p_{B3}}{\partial y} \right|_{y=y_1} = \frac{k_{B2}}{\mu} \left. \frac{\partial p_{B2}}{\partial y} \right|_{y=y_1} \tag{7}$$

Considering the fluid flow sequentially from the un-stimulated region to the stimulated region, the diffusivity equation to describe the flow process in stimulated region defined Region 2 can be written similarly as

$$\frac{\partial^2 p_{B2}}{\partial x^2} + \frac{\partial^2 p_{B2}}{\partial y^2} + \frac{\partial^2 p_{B2}}{\partial z^2} = \frac{(\phi\mu c_t)_{B2}}{k_{B2}} \frac{\partial p_{B2}}{t} \tag{8}$$

For Region 2, the initial condition is identical.

$$p_{B2}(x, y, z, 0) = p_i \tag{9}$$

The bottom of Region 2 is the horizontal wellbore, which is defined as an impermeable boundary. Therefore, the outer boundary condition is expressed as

$$\left. \frac{\partial p_{B2}}{\partial y} \right|_{y=y_0} = 0 \tag{10}$$

$$\left. \frac{\partial p_{B2}}{\partial z} \right|_{z=z_0, z_e} = 0 \tag{11}$$

Due to the symmetry, another outer boundary condition is similar to Equation (6):

$$\left. \frac{\partial p_{B2}}{\partial x} \right|_{x=x_e} = 0 \tag{12}$$

Because the stimulated region is connected to the hydraulic fracture region and the unstimulated region, the inner boundary condition of Region 2 can be written as

$$\frac{k_{B2}}{\mu} \left. \frac{\partial p_{B2}}{\partial y} \right|_{y=y_1} = \frac{k_{B3}}{\mu} \left. \frac{\partial p_{B3}}{\partial y} \right|_{y=y_1} \tag{13}$$

$$\frac{k_{B2}}{\mu} \left. \frac{\partial p_{B2}}{\partial x} \right|_{x=x_0} = \frac{k_{B1}}{\mu} \left. \frac{\partial p_{B1}}{\partial x} \right|_{x=x_0} \tag{14}$$

Similarly, the equations to describe the fluid flow in hydraulic fracture region defined as Region 1 can be expressed as

$$\frac{\partial^2 p_{B1}}{\partial x^2} + \frac{\partial^2 p_{B1}}{\partial y^2} + \frac{\partial^2 p_{B1}}{\partial z^2} = \frac{(\phi\mu c_t)_{B1}}{k_{B1}} \frac{\partial p_{B1}}{t} \tag{15}$$

The hydraulic fracture region is sole connection to well and the production is under constant bottom-hole pressure. Therefore, the initial conditions for Region 1 is given by

$$p_{B1}(x, y, z, 0) = p_i \tag{16}$$

$$p_{B1}(x, y = y_0, z, t) = p_{wf} \tag{17}$$

There is no fluid flow beyond the tip of hydraulic fracture and the location of $x = 0$. The boundary conditions can be written as

$$\left. \frac{\partial p_{B1}}{\partial x} \right|_{x=0} = 0 \tag{18}$$

$$\left. \frac{\partial p_{B1}}{\partial y} \right|_{y=y_1} = 0 \tag{19}$$

$$\left. \frac{\partial p_{B1}}{\partial z} \right|_{z=z_0, z_e} = 0 \tag{20}$$

The hydraulic fracture region is connected to the stimulated region. The flow is continuous at $x = x_0$.

$$\left. \frac{k_{B1}}{\mu} \frac{\partial p_{B1}}{\partial x} \right|_{x=x_0} = \left. \frac{k_{B2}}{\mu} \frac{\partial p_{B2}}{\partial x} \right|_{x=x_0} \tag{21}$$

Model 2: Based on Stalgorova and Matter’s conceptual model

Comparing the two concept models, we can find that the flow direction in the two regions is vertical in Model 1 and parallel in Model 2. In other words, the mathematical model developed for Model 2 is nearly alike that of Model 1 except for the boundary conditions. Similarly, the governing equation for un-stimulated region defined as Region 3 is expressed as

$$\frac{\partial^2 p_{S3}}{\partial x^2} + \frac{\partial^2 p_{S3}}{\partial y^2} + \frac{\partial^2 p_{S3}}{\partial z^2} = \frac{(\phi\mu c_t)_{S3}}{k_{S3}} \frac{\partial p_{S3}}{t} \tag{22}$$

The pressure in Region 3 is the initial reservoir pressure when $t = 0$.

$$p_{S3}(x, y, z, 0) = p_i \tag{23}$$

As the boundary is defined as no-flow at the top and bottom of the reservoir, meanwhile, both ends of the y -direction can also be regarded as a no-flow boundary in Model 2.

$$\left. \frac{\partial p_{S3}}{\partial y} \right|_{y=y_{wf}, y_e} = 0 \tag{24}$$

$$\left. \frac{\partial p_{S3}}{\partial z} \right|_{z=z_0, z_e} = 0 \tag{25}$$

Because of the symmetry, there is no fluid flow that occurs at $x = x_2$.

$$\left. \frac{\partial p_{S3}}{\partial x} \right|_{x=x_2} = 0 \tag{26}$$

There is the contact surface between the unstimulated region and the stimulated region. Therefore, the last boundary condition can be given by

$$\frac{k_{S3}}{\mu} \frac{\partial p_{S3}}{\partial x} \Big|_{x=x_1} = \frac{k_{S2}}{\mu} \frac{\partial p_{S2}}{\partial x} \Big|_{x=x_1} \tag{27}$$

The flow in stimulated region defined as Region 2 can also be expressed by a series of equations. Firstly, the diffusivity equation for fluid flow in Region 2 can be expressed as

$$\frac{\partial^2 p_{S2}}{\partial x^2} + \frac{\partial^2 p_{S2}}{\partial y^2} + \frac{\partial^2 p_{S2}}{\partial z^2} = \frac{(\phi\mu c_t)_{S2}}{k_{S2}} \frac{\partial p_{S2}}{t} \tag{28}$$

Similarly, the initial condition is identical to Region 3.

$$p_{S2}(x, y, z, 0) = p_i \tag{29}$$

The bottom of Region 2 is the horizontal wellbore, which is defined as impermeable boundary. Therefore, we can obtain the outer boundary conditions as follows

$$\frac{\partial p_{S2}}{\partial y} \Big|_{y=y_{wf}, y_e} = 0 \tag{30}$$

$$\frac{\partial p_{S2}}{\partial z} \Big|_{z=z_0, z_e} = 0 \tag{31}$$

According to the continuity of flux and pressure in the interface, the inner boundary condition of Region 2 can be given by

$$\frac{k_{S2}}{\mu} \frac{\partial p_{S2}}{\partial x} \Big|_{x=x_1} = \frac{k_{S3}}{\mu} \frac{\partial p_{S3}}{\partial x} \Big|_{x=x_1} \tag{32}$$

$$\frac{k_{S2}}{\mu} \frac{\partial p_{S2}}{\partial x} \Big|_{x=x_0} = \frac{k_{S1}}{\mu} \frac{\partial p_{S1}}{\partial x} \Big|_{x=x_0} \tag{33}$$

Similarly, the equations to describe the fluid flow in hydraulic fracture region defined as Region 1 can be expressed as

$$\frac{\partial^2 p_{S1}}{\partial x^2} + \frac{\partial^2 p_{S1}}{\partial y^2} + \frac{\partial^2 p_{S1}}{\partial z^2} = \frac{(\phi\mu c_t)_{S1}}{k_{S1}} \frac{\partial p_{S1}}{t} \tag{34}$$

The initial condition is exactly same as Equation (29). Meanwhile, the pressure at $y = y_{wf}$ is the bottom-hole pressure and remains constant.

$$p_{S1}(x, y, z, 0) = p_i \tag{35}$$

$$p_{S1}(x, y = y_{wf}, z, t) = p_{wf} \tag{36}$$

There is also no fluid flow beyond the tip of hydraulic fracture and at top and bottom of the reservoir. The outer boundary conditions can be written as

$$\frac{\partial p_{S1}}{\partial x} \Big|_{x=0} = 0 \tag{37}$$

$$\frac{\partial p_{S1}}{\partial y} \Big|_{y=y_1} = 0 \tag{38}$$

$$\left. \frac{\partial p_{S1}}{\partial z} \right|_{z=z_0, z_e} = 0 \tag{39}$$

There is an interface between the stimulated region and the hydraulic fracture region. The flux is considered to be continuous, and then the boundary condition is expressed as

$$\left. \frac{k_{S1}}{\mu} \frac{\partial p_{S1}}{\partial x} \right|_{x=x_0} = \left. \frac{k_{S2}}{\mu} \frac{\partial p_{S2}}{\partial x} \right|_{x=x_0} \tag{40}$$

3. Model Derivation

The above equations to describe fluid flow process in these two models are all PDEs. Prior to deriving the analytical solution, the system of PDEs must be transformed into ODEs. In this section, the new approaches, i.e., the integral transform and average pressure substitution, are used to solve the above equations in real-time space. Firstly, Equation (1) in the Model 1 can be rewritten as

$$\int_{x_0}^{x_e} \int_{y_1}^{y_2} \int_{z_0}^{z_e} \frac{\partial}{\partial x} \left(\frac{\partial P_{B3}}{\partial x} \right) dx dy dz + \int_{x_0}^{x_e} \int_{y_1}^{y_2} \int_{z_0}^{z_e} \frac{\partial}{\partial y} \left(\frac{\partial P_{B3}}{\partial y} \right) dx dy dz + \int_{x_0}^{x_e} \int_{y_1}^{y_2} \int_{z_0}^{z_e} \frac{\partial}{\partial z} \left(\frac{\partial P_{B3}}{\partial z} \right) dx dy dz = \frac{(\phi \mu c_t)_{B3}}{k_{B3}} \frac{\partial}{\partial t} \int_{x_0}^{x_e} \int_{y_1}^{y_2} \int_{z_0}^{z_e} P_{B3} dx dy dz \tag{41}$$

In order to obtain a simplified equation, the average pressure and effective pore volume are defined as

$$\overline{p_{B3}} = \frac{\iiint p_{B3}}{\iiint dx dy dz} = \frac{\iiint p_{B3}}{V_{b,B3}} \tag{42}$$

$$V_{p,B3} = \phi V_{b,B3} \tag{43}$$

Based on the above definitions, Equation (41) can be re-written as

$$\int_{y_1}^{y_2} \int_{z_0}^{z_e} \left(\left. \frac{\partial p_{B3}}{\partial x} \right|_{x_e} - \left. \frac{\partial p_{B3}}{\partial x} \right|_{x_0} \right) dy dz + \int_{x_0}^{x_e} \int_{z_0}^{z_e} \left(\left. \frac{\partial p_{B3}}{\partial y} \right|_{y_2} - \left. \frac{\partial p_{B3}}{\partial y} \right|_{y_1} \right) dx dz + \int_{x_0}^{x_e} \int_{y_1}^{y_2} \left(\left. \frac{\partial p_{B3}}{\partial z} \right|_{z_e} - \left. \frac{\partial p_{B3}}{\partial z} \right|_{z_0} \right) dx dy = \frac{(\phi \mu c_t)_{B3} V_{b,B3}}{k_{B3}} \frac{d\overline{p_{B3}}}{dt} \tag{44}$$

Substituting the initial conditions and boundary conditions, Equation (44) simplifies to

$$-\int_{x_0}^{x_e} \int_{z_0}^{z_e} \left(\left. \frac{\partial p_{B3}}{\partial y} \right|_{y_1} \right) dx dz = \frac{(\phi \mu c_t)_{B3} V_{b,B3}}{k_{B3}} \frac{d\overline{p_{B3}}}{dt} \tag{45}$$

According to Darcy’s law

$$q_{B3} = \int_{x_0}^{x_e} \int_{z_0}^{z_e} \left(\frac{k_{B3}}{\mu} \left. \frac{\partial p_{B3}}{\partial y} \right|_{y_1} \right) dx dz \tag{46}$$

Therefore, Equation (45) can be rewritten as shown below

$$(c_t V_p)_{B3} \frac{d\overline{p_{B3}}}{dt} = -q_{B3} \tag{47}$$

Similarly, the simplified ODEs for Region 2 and Region 1 of Model 1 can be expressed as

$$(c_t V_p)_{B2} \frac{d\overline{p_{B2}}}{dt} = -q_{B2} + q_{B3} \tag{48}$$

$$(c_t V_p)_{B1} \frac{d\overline{p_{B1}}}{dt} = -q_{B1} + q_{B2} \tag{49}$$

For Model 2, Equation (22) can also be rewritten as

$$\int_{y_{wf}}^{y_e} \int_{z_0}^{z_e} \left(\left. \frac{\partial p_{S3}}{\partial x} \right|_{x_2} - \left. \frac{\partial p_{S3}}{\partial x} \right|_{x_1} \right) dydz + \int_{x_1}^{x_2} \int_{z_0}^{z_e} \left(\left. \frac{\partial p_{S3}}{\partial y} \right|_{y_e} - \left. \frac{\partial p_{S3}}{\partial y} \right|_{y_{wf}} \right) dx dz + \int_{x_1}^{x_2} \int_{y_{wf}}^{y_e} \left(\left. \frac{\partial p_{S3}}{\partial z} \right|_{z_e} - \left. \frac{\partial p_{S3}}{\partial z} \right|_{z_0} \right) dx dy = \frac{(\phi\mu c_t)_{S3} V_{b,S3}}{k_{S3}} \frac{d\bar{p}_{S3}}{dt} \quad (50)$$

Substituting the initial conditions and boundary conditions, Equation (50) can be simplified as

$$- \int_{y_{wf}}^{y_e} \int_{z_0}^{z_e} \left(\left. \frac{\partial p_{S3}}{\partial x} \right|_{x_1} \right) dydz = \frac{(\phi\mu c_t)_{S3} V_{b,S3}}{k_{S3}} \frac{d\bar{p}_{S3}}{dt} \quad (51)$$

Note that

$$q_{S3} = \int_{y_{wf}}^{y_e} \int_{z_0}^{z_e} \left(\frac{k_{S3}}{\mu} \left. \frac{\partial p_{S3}}{\partial x} \right|_{x_1} \right) dydz \quad (52)$$

Substituting Equation (52) into Equation (51) results in

$$(c_t V_p)_{S3} \frac{d\bar{p}_{S3}}{dt} = -q_{S3} \quad (53)$$

Similarly, the simplified ODEs for Region 2 and Region 1 of Model 2 can be expressed as

$$(c_t V_p)_{S2} \frac{d\bar{p}_{S2}}{dt} = -q_{S2} + q_{S3} \quad (54)$$

$$(c_t V_p)_{S1} \frac{d\bar{p}_{S1}}{dt} = -q_{S1} + q_{S2} \quad (55)$$

Comparing Equations (47)–(49) with Equations (53)–(55), we can find that the form of these equations are exactly the same, which also means that the obtained analytical solution through the new approach is identical for the two models. The next step is to replace the average pressure and the general form of average pressure representing the relationship between the pressure and the dimensionless flow rate, which can be expressed as [23]

$$\bar{p} = p_{wf} + \frac{4}{\pi^2} (p_i - p_{wf}) \sum_{n=1}^{\infty} \frac{q_{Dn}}{(2n - 1)^2} \quad (56)$$

The linear flow process is from Region 3 to Region 2 and then Region 1, sequentially. Therefore, the average pressure in Region 1, Region 2 and Region 3 can be written, respectively, as

$$\bar{p}_1 = p_{wf} + \frac{q_1}{J} \sum_{n=1}^{\infty} \frac{q_{Dn1}}{(2n - 1)^2} \quad (57)$$

$$\bar{p}_2 = \bar{p}_1 + \frac{q_2}{T_{21}} \sum_{n=1}^{\infty} \frac{q_{Dn2}}{(2n - 1)^2} \quad (58)$$

$$\bar{p}_3 = \bar{p}_2 + \frac{q_3}{T_{32}} \sum_{n=1}^{\infty} \frac{q_{Dn3}}{(2n - 1)^2} \quad (59)$$

where q_{Dn1} , q_{Dn2} and q_{Dn3} are the dimensionless production rate from the n -th mode in Region 1, Region 2 and Region 3, respectively. q_1 , q_2 and q_3 and \bar{p}_1 , \bar{p}_2 and \bar{p}_3 are the initial production rate and average pressure in Region 1, Region 2 and Region 3, respectively. The productivity index is represented by J and the transmissibility between two regions are represented by T_{21} and T_{32} , which can be defined as $J = \frac{\pi^2}{4} \frac{q_1}{p_i - p_{wf}}$, $T_{21} = \frac{\pi^2}{4} \frac{q_2}{p_i - \bar{p}_1}$ and $T_{32} = \frac{\pi^2}{4} \frac{q_3}{p_i - \bar{p}_2}$.

Substituting the general equations of average pressure Equations (57)–(59) into Equations (47)–(49) or Equations (53)–(55), the ODEs in three regions can be rewritten as

$$\sum_{n=1}^{\infty} \frac{dq_{n1}}{dt} = \frac{1}{\tau_1} \sum_{n=1}^{\infty} (2n-1)^2 q_{n2}(t) - \frac{1}{\tau_1} \sum_{n=1}^{\infty} (2n-1)^2 q_{n1}(t) \tag{60}$$

$$\sum_{n=1}^{\infty} \frac{dq_{n2}}{dt} = \frac{1}{\tau_2} \sum_{n=1}^{\infty} (2n-1)^2 q_{n3}(t) - \left(\frac{1}{\tau_2} + \frac{T_{21}}{J\tau_1}\right) \sum_{n=1}^{\infty} (2n-1)^2 q_{n2}(t) + \frac{T_{21}}{J\tau_1} \sum_{n=1}^{\infty} (2n-1)^2 q_{n1}(t) \tag{61}$$

$$\sum_{n=1}^{\infty} \frac{dq_{n3}}{dt} = -\left(\frac{1}{\tau_3} + \frac{T_{21}}{T_{32}\tau_2}\right) \sum_{n=1}^{\infty} (2n-1)^2 q_{n3}(t) - \frac{T_{21}}{T_{32}\tau_2} \sum_{n=1}^{\infty} (2n-1)^2 q_{n2}(t) \tag{62}$$

where τ_1 , τ_2 and τ_3 indicate the linear flow time in Region 1, Region 2 and Region 3, respectively, which can be defined as $\tau_1 = \frac{(c_t V_p)_1}{J}$, $\tau_2 = \frac{(c_t V_p)_2}{T_{21}}$ and $\tau_3 = \frac{(c_t V_p)_3}{T_{32}}$.

The initial oil rate depends on the flow rate from Region 1. Therefore, the initial conditions for three regions can be expressed as

$$q_1(t=0) = q_i \tag{63}$$

$$q_2(t=0) = 0 \tag{64}$$

$$q_3(t=0) = 0 \tag{65}$$

Solving Equations (60)–(62) by substituting Equations (63)–(65), the production rate for n -th mode can be obtained as

$$q_{n1} = (2n-1)^2 \left(\beta_3 r_3 q_i e^{(2n-1)^2 \lambda_1 t} - \beta_2 r_6 q_i e^{(2n-1)^2 \lambda_2 t} + \beta_1 r_9 q_i e^{(2n-1)^2 \lambda_3 t} \right) \tag{66}$$

where λ_1 , λ_2 and λ_3 are three eigenvalues and $r_1 \sim r_9$ represent the nine elements in three eigenvectors. And β_1 , β_2 and β_3 are the combination of parameters, which can be expressed as $\beta_1 = \frac{r_1(r_1 r_5 - r_2 r_4)}{(r_1 r_9 - r_3 r_7)(r_1 r_5 - r_2 r_4) - (r_1 r_6 - r_3 r_4)(r_1 r_8 - r_2 r_7)}$, $\beta_2 = \frac{r_1 r_8 - r_2 r_7}{r_1 r_5 - r_2 r_4} \beta_1$, $\beta_3 = \frac{\beta_2 r_4 r_7}{r_1} \beta_1$.

The production rate q_1 is the summation of all production rate terms. After many mathematical manipulations, the analytical solution can be obtained by simplifying Equation (66).

$$q_1 = (\beta_3 r_3 q_i e^{\lambda_1 t} - \beta_2 r_6 q_i e^{\lambda_2 t} + \beta_1 r_9 q_i e^{\lambda_3 t}) + \frac{\sqrt{\pi} \beta_3 r_3 q_i}{4\sqrt{|\lambda_1|t}} \operatorname{erfc}\left(3\sqrt{|\lambda_1|t}\right) - \frac{\sqrt{\pi} \beta_2 r_6 q_i}{4\sqrt{|\lambda_2|t}} \operatorname{erfc}\left(3\sqrt{|\lambda_2|t}\right) + \frac{\sqrt{\pi} \beta_1 r_9 q_i}{4\sqrt{|\lambda_3|t}} \operatorname{erfc}\left(3\sqrt{|\lambda_3|t}\right) \tag{67}$$

Obviously, we can obtain that the oil rate depends on several variables from Equations (60)–(62), i.e., the linear flow time (τ_1 , τ_2 , τ_3) in Region 1, Region 2 and Region 3, productivity index J , two transmissibility T_{21} and T_{32} and initial production rate q_i . By fitting Equation (67) to the target data, the several variables can be obtained when the desired match is achieved. In addition, the analytical solution with output variables can be further used for production prediction.

4. Model Validation

The general analytical solution for two typical configurations has been derived. Therefore, the main objective of this section is to verify the accuracy of the analytical solution by constructing two numerical models based on the previous two physical configurations. Considering the assumption of symmetry, the two numerical models are both one quarter and are constructed with 27 grid cells in the x -direction, 50 grid cells in the y -direction and only 1 grid cell in the z -direction, which is illustrated in Figure 2. Due to the vast difference in the width dimensions of fractures and matrix, the additional refinement scheme around the hydraulic fractures and near the boundaries of discretized regions is employed, enhanc-

ing stability of the numerical solution while accurately capturing the transient responses within the fractures. The blue area represents the stimulated region (Region 2), while the gray area is the unstimulated region (Region 3). The hydraulic fracture region (Region 1) is relatively small and is represented by the grids in the first column. Furthermore, Regions 1 and 2 and Regions 2 and 3 are individually connected to ensure sequential flow among three regions. The input parameters for the two numerical models are summarized in Table 1.

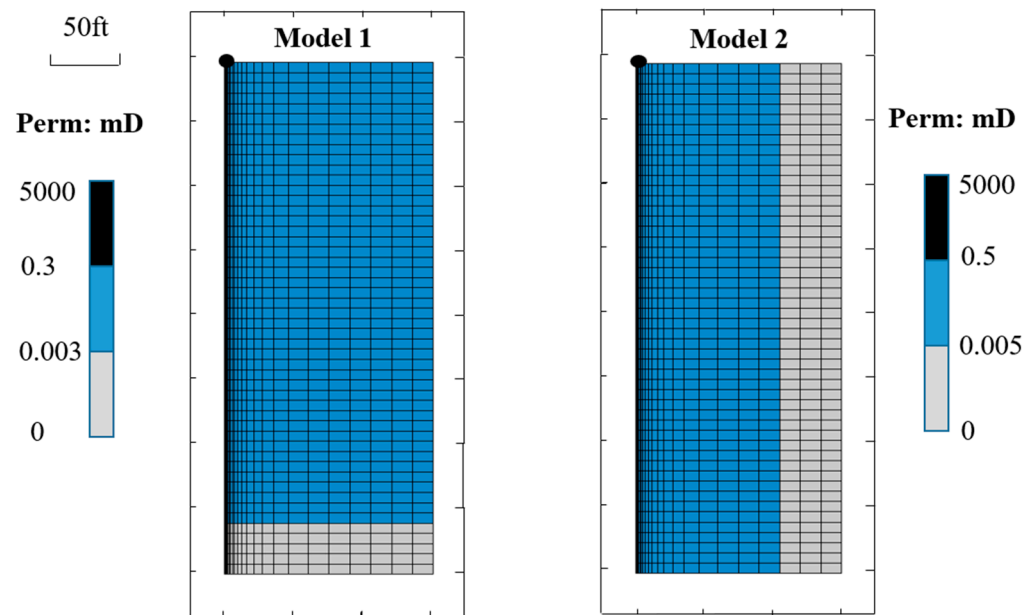


Figure 2. Schematic of the reservoir grids for two numerical models with typical configurations.

Table 1. Input parameters for the numerical models.

Parameter	Model 1	Model 2
	Value	
Model dimension (X × Y × Z) (ft)	150 × 400 × 10	150 × 400 × 10
Initial pressure (psi)	2500	2500
Bottom-hole pressure (psi)	500	500
Viscosity (cp)	0.0174	0.0174
Compressibility (10 ⁻⁵ psi)	9.75	9.75
Porosity	0.06	0.06
Permeability of hydraulic fracture	5000	5000
Permeability in Region 3 (mD)	0.003	0.005
Permeability in Region 2 (mD)	0.3	0.5

The comparison results between two numerical models and the analytical solution are presented in Figure 3. The black dots indicate the results of oil rate over time as calculated by the numerical models, while the red lines indicate the results of the analytical solution. Obviously, the fitting results are excellent. As shown in Figure 3a,b, four flow regimes are both identified. Because of the high-velocity flow in the hydraulic fracture region (Region 1), the two flow regimes happened in Region 1 are not presented. The first regime can be diagnosed as a transient linear flow in Region 2, which also corresponds to the $-1/2$ straight line presented on the log-log plot. Region 2 is the stimulated region with relatively high permeability, which is significant for short-term production of the reservoir, so the linear flow time in this region is 418 days in Model 1 and 244 days in Model 2, respectively. The exponential curve representing the second flow regime indicates that the pressure wave reaches the boundary of Region 2. As for the third flow regime, it indicates the transient linear flow in Region 3 with a low-permeability matrix, which contributes

significantly to long-term production, so the linear flow time in this region is 1869 days in Model 1 and 1389 days in Model 2, respectively. Lastly, the fourth flow regime is outer boundary-dominated flow. The six output parameters from the fit to two numerical models are listed in Table 2.

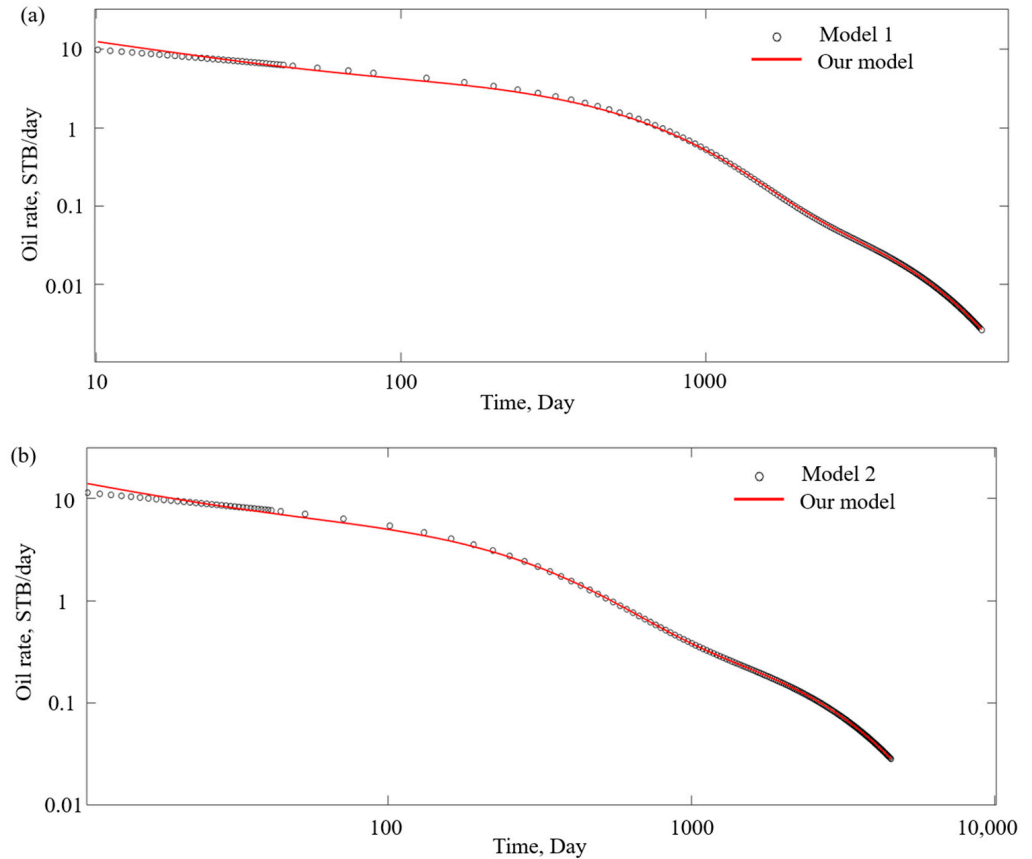


Figure 3. Comparative results with two numerical models.

Table 2. Output parameters obtained from the analytical solution for validation against two numerical models.

	Model 1	Model 2
Parameter	Value	
τ_1 (days)	1.2×10^{-4}	1.4×10^{-4}
τ_2 (days)	418	244
τ_3 (days)	1869	1389
T_{21}/J	0.012	0.01
T_{32}/T_{21}	0.022	0.065
q_i (STB/day)	10.96	12.02

5. Application to Field Cases

The accuracy of the new analytical solution has been verified against the numerical models based on two typical configurations. Before applying the analytical solution to field cases, a workflow for processing the raw field data must be developed because the type and number of flow regimes observed in a field data plot depends on the relative magnitude of the well and reservoir properties. Meanwhile, the dominance of linear flow regime observed in field data could result from (1) production from fractures whose lengths extend to reservoir boundaries, (2) transient drainage of low-permeability matrix blocks into adjoining fractures, and (3) linear shape of certain reservoirs [24]. Therefore, flow pattern analysis and history matching for production data from fractured reservoirs are

necessary. One onshore field case and one offshore field case are extracted for production prediction according to the main workflow. The five main steps are listed as follows:

- Make a log–log plot of oil rate versus production time.
- Diagnose the flow regimes.
- Apply analytical solution to the production data.
- Output the six parameters after obtaining the desired matching.
- Predict the future production rate with the obtained parameters.

Onshore field case. Well O is one of tight oil wells located at Elm Coulee Field in eastern Montana, whose data are from the paper published by Kabir et al. [25] in 2011. Well O was selected primarily because of its relatively long production history and the availability of high quality pressure data. The well has been on production for 350 days at constant BHPs. Firstly, the original oil rate versus production time on the log–log plot can be obtained, which exhibits a $-1/2$ straight line and a nearly unit-slope line indicating linear flow and boundary-dominated flow in Figure 4a. Since the linear flow lasts for nearly 200 days, this linear flow can be diagnosed as the transient linear flow in stimulated region. Meanwhile, the boundary-dominated flow indicates that the pressure wave has reached the boundary of stimulated region. Following the work flow, we apply our analytical model to the field data. The result of production-rate history match and forecast are shown in Figure 4b on a log–log plot. The green marks (history match) and the red marks (field data) reach a high degree of fit except for the noisy data. Thus, we summarized the output parameters obtained from the history-match exercise in Table 3. After substituting the output parameters into the analytical solution, we can predict the future production rate until 3000 days, which are shown using black marks. As shown in Figure 4b, two more flow regions can be identified, which is the typical linear flow and boundary-dominated flow in the unstimulated region. The supply from the ultra-tight matrix can last for a long time, which is critical to the cumulative production of a tight oil well.

Table 3. Output parameters obtained from the analytical solution for application in two field cases.

Parameter	Well O	Volve Field
	Value	
τ_1	0.003 (days)	5×10^{-6} (Months)
τ_2	197(days)	14 (Months)
τ_3	2100 (days)	460 (Months)
T_{21}/J	0.203	0.0729
T_{32}/T_{21}	0.049	0.0045
q_i	1200 (STB/day)	1780 (MSTB/month)

Offshore field case. This offshore oil field data is obtained from Wang’s published paper [26]. The production wells are drilled in the Volve oil field located in the central part of the North Sea. The target formation is tight sandstone of Middle Jurassic age at the depth of about 3000m below sea level. The field was developed in early 2008 and was in operation for roughly nine years. As illustrated in Figure 5a, the monthly oil rate versus production time is presented on the log–log plot with a $-1/2$ straight line. The linear flow time lasts for nearly 70 months, which means the flow regime can be diagnosed as transient flow in unstimulated region. After fitting our analytical solution to the field data, the results of history matching and production prediction are shown in Figure 5b. A great matching degree can be obtained, and six model output parameters are summarized in Table 3. Furthermore, we can predict the further monthly oil rate until 2500 months. We can observe that the monthly oil rate will be below 500 MSTB/month in the ninth year. That would explain why this oil field was decommissioned in 2016 combined with the high cost of offshore oil extraction.

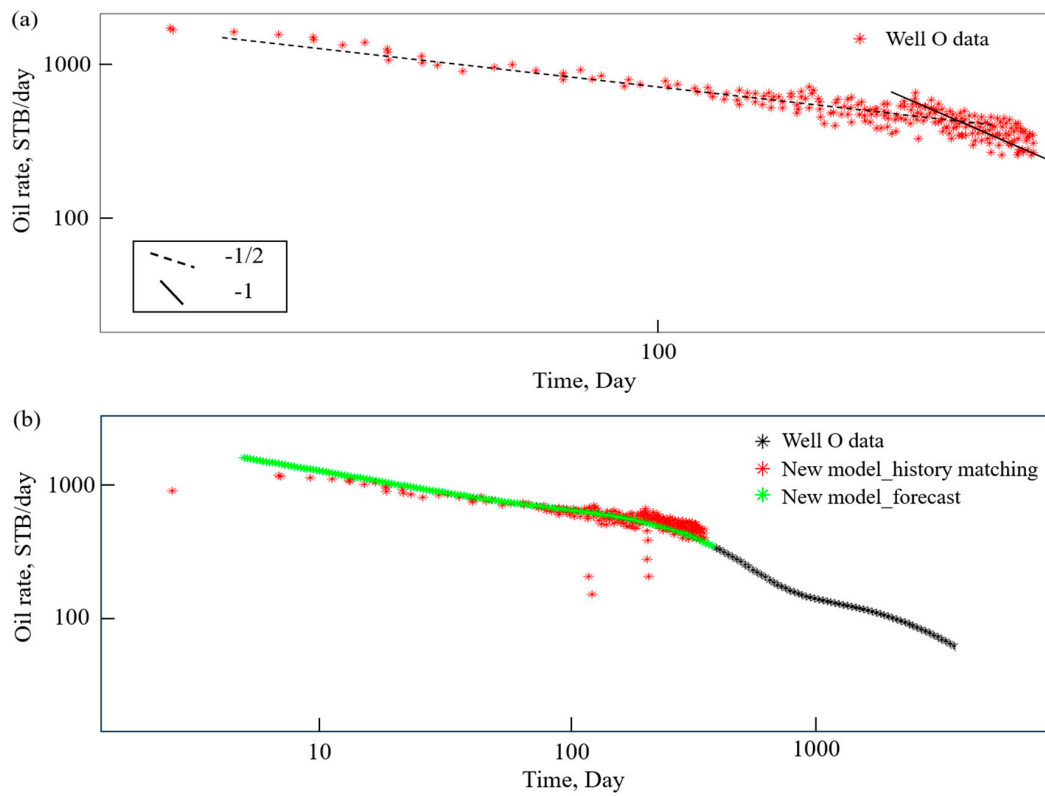


Figure 4. Production analysis in Well O. (a) Actual oil rate on the log–log plot; (b) the history matching and forecasting results on the log–log plot.

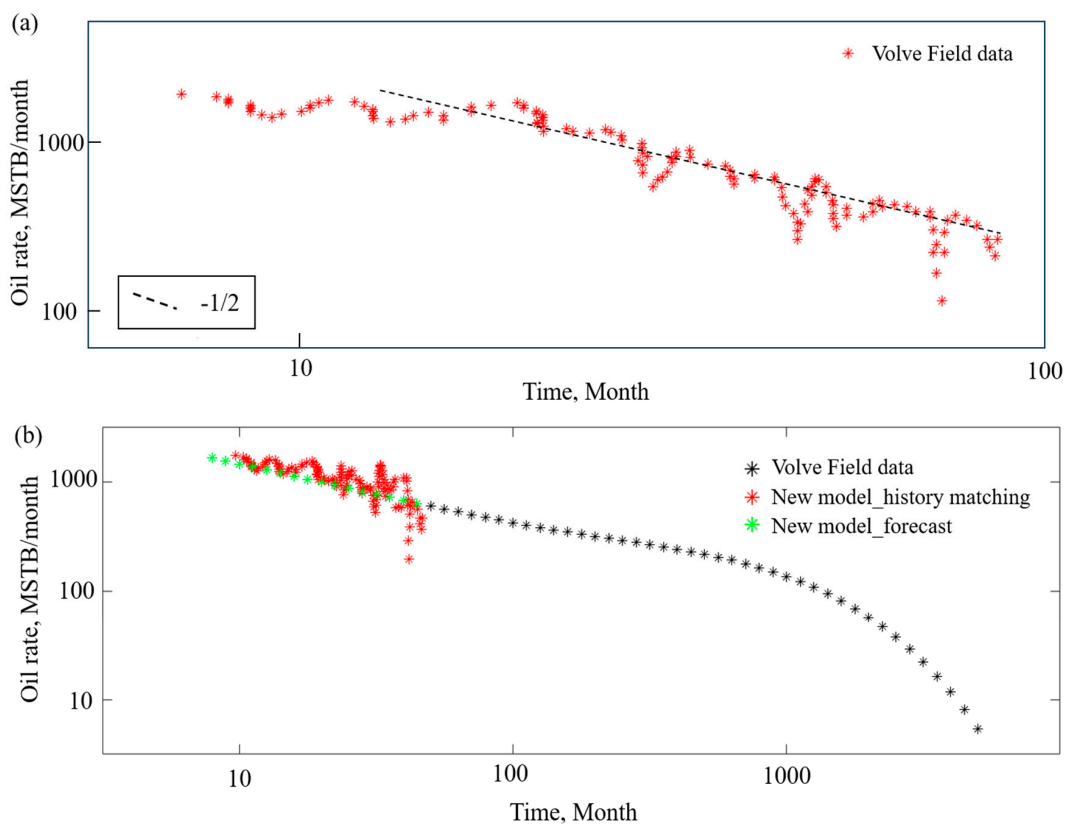


Figure 5. Production analysis in Volve oil field. (a) Actual oil rate on the log–log plot; (b) the history matching and forecasting results on the log–log plot.

6. Conclusions

In this study, we adopt a new approach to derive a general analytical solution in real-time space for two typical tri-linear physical configurations. Numerical models with identical physical configurations had been used to validate the accuracy of the analytical solution and then a production data analysis had been carried out to analyze short-term and long-term performance of two field cases based on the developed workflow. The specific conclusions can be drawn:

- Through bypassing the complex Laplace transform solution, the analytical solution is derived in real-time space and directly presents the oil-rate-versus-production-time relationship. Therefore, it is more convenient in field applications.
- The derived analytical solution is not only applicable to unconventional reservoirs without the region beyond the hydraulic fractures, but can also consider the contribution from the region beyond the hydraulic fractures because of the excellent agreement with two numerical models.
- The diagnosis of transient linear flow in offshore and onshore tight oilfields is critical for production data analysis. The same slope straight line may represent the different fluid-transfer mechanism, and the linear flow in unstimulated region cannot be ignored, which represents a significant contribution to long-term production.

Author Contributions: Methodology, K.Q.; Software, X.C., G.L. and S.W.; Investigation, K.F.; Resources, K.F. and J.L.; Data curation, K.F. and X.C.; Writing—original draft, K.Q.; Writing—review & editing, G.L., S.W. and R.N. All authors have read and agreed to the published version of the manuscript.

Funding: This study was supported by Basic Research Project from Jiangmen Science and Technology Bureau (Grant Nos. 2220002000356), China University of Petroleum (Beijing) (Grand No. 2462023BJRC007), National Natural Science Foundation of China (Grant Nos. 72140008) and The Guangdong Basic and Applied Basic Research Foundation (No. 2022A1515110376).

Institutional Review Board Statement: Not applicable.

Informed Consent Statement: Not applicable.

Data Availability Statement: All data have been provided in the paper.

Conflicts of Interest: We declare that we have no conflict of interest.

References

1. Zhao, Z.; Hou, L.; Luo, X.; Chi, Y.; Pang, Z.; Lin, S.; Zhang, L.; Liu, B. Heat-induced pore structure evolution in the Triassic chang 7 shale, Ordos basin, China: Experimental simulation of in situ conversion process. *J. Mar. Sci. Eng.* **2023**, *11*, 1363. [CrossRef]
2. Masoud, S.; Sohrab, Z.; Stephen, B. Molecular dynamics simulations in reservoir analysis of offshore petroleum reserves: A systematic review of theory and applications. *Earth-Sci. Rev.* **2019**, *192*, 194–213.
3. U.S. Energy Information Administration. Offshore Production Nearly 30% of Global Crude Oil Output in 2015. 2016. Available online: <https://go.gale.com/ps/i.do?p=EAIM&u=anon~b06c66bc&id=GALE|A467716915&v=2.1&it=r&sid=sitemap&asid=c037960b> (accessed on 1 October 2016).
4. Abassi, M.; Sharifi, M.; Kazemi, A. Development of new analytical model for series and parallel triple porosity models and providing transient shape factor between different regions. *J. Hydrol.* **2019**, *574*, 683–698. [CrossRef]
5. Lei, G.; Liu, T.; Liao, Q.; He, X. Estimating permeability of porous media from 2D digital images. *J. Mar. Sci. Eng.* **2023**, *11*, 1614. [CrossRef]
6. Fathy, D.; El-Balkiemy, A.F.; Makled, W.A.; Hosny, A.M. Organic geochemical signals of Paleozoic rocks in the southern Tethys, Siwa basin, Egypt: Implications for source rock characterization and petroleum system. *Phys. Chem. Earth* **2023**, *130*, 103393. [CrossRef]
7. Benetatos, C.; Catania, F.; Giglio, G.; Pirri, C.F.; Raeli, A.; Scaltrito, L.; Serazio, C.; Verga, F. Workflow for the validation of geomechanical simulations through seabed monitoring for offshore underground activities. *J. Mar. Sci. Eng.* **2023**, *11*, 1387. [CrossRef]
8. Clarkson, C.R. Production data analysis of unconventional gas wells: Review of theory and best practices. *Int. J. Coal Geol.* **2013**, *110*, 101–146. [CrossRef]
9. Dejam, M.; Hassanzadeh, H.; Chen, Z. Semi-analytical solution for pressure transient analysis of a hydraulically fractured vertical well in a bounded dual-porosity reservoir. *J. Hydrol.* **2018**, *565*, 289–301. [CrossRef]

10. Wei, S.; Xia, Y.; Jin, Y.; Chen, M.; Chen, K. Quantitative study in shale gas behaviors using a coupled triple-continuum and discrete fracture model. *J. Pet. Sci. Eng.* **2019**, *174*, 49–69. [\[CrossRef\]](#)
11. Rao, X.; Xin, L.; He, Y.; Fang, X.; Gong, R.; Wang, F.; Zhao, H.; Shi, J.; Xu, Y.; Dai, W. Numerical simulation of two-phase heat and mass transfer in fractured reservoirs based on projection-based embedded discrete fracture model (pEDFM). *J. Pet. Sci. Eng.* **2022**, *208*, 109323. [\[CrossRef\]](#)
12. Ahmadi, S.; Khormali, A. Optimization of the corrosion inhibition performance of 2-mercaptobenzothiazole for carbon steel in HCl media using response surface methodology. *Fuel* **2024**, *357*, 129783. [\[CrossRef\]](#)
13. Qiu, K.X.; Li, J.; Chen, D. Optimized long short-term memory (LSTM) network for performance prediction in unconventional reservoirs. *Energy Rep.* **2022**, *8*, 15436–15445. [\[CrossRef\]](#)
14. Khormali, A. Effect of water cut on the performance of an asphaltene inhibitor package: Experimental and modeling analysis. *Petrol. Sci. Technol.* **2022**, *40*, 2890–2906. [\[CrossRef\]](#)
15. El-Banbi, A. Analysis of Tight Gas Well Performance. Ph.D. Thesis, Texas A&M University, College Station, TX, USA, 1998.
16. Bello, R.O. Rate Transient Analysis in Shale Gas Reservoirs with Transient Linear Behavior. Ph.D. Thesis, Texas A&M University, College Station, TX, USA, 2009.
17. Brown, M.; Ozkan, E.; Raghavan, R.; Kazemi, H. Practical solutions for pressure-transient responses of fractured horizontal wells in unconventional shale reservoirs. *SPE Res. Eval. Eng.* **2011**, *14*, 663–676. [\[CrossRef\]](#)
18. Stalgorova, E.; Mattar, L. Practical analytical model to simulate production of horizontal wells with branch fractures. In Proceedings of the SPE Canadian Unconventional Resources Conference, Calgary, AB, Canada, 30 October–1 November 2012.
19. Ogunyomi, B.A.; Patzek, T.W.; Lake, L.W.; Kabir, C.S. History matching and rate forecasting in unconventional oil reservoirs with an approximate analytical solution to the double-porosity model. *SPE Res. Eval. Eng.* **2016**, *19*, 70–82. [\[CrossRef\]](#)
20. Qiu, K.X.; Li, H. A New Analytical Solution of the Triple-Porosity Model for History Matching and Performance Forecasting in Unconventional Oil Reservoirs. *SPE J.* **2018**, *23*, 2060–2079. [\[CrossRef\]](#)
21. Qiu, K.X. A practical analytical model for performance prediction in unconventional gas reservoir. *Front. Earth Sci.* **2023**, *11*, 1143541. [\[CrossRef\]](#)
22. Stehfest, H. Algorithm 368: Numerical Inversion of Laplace transforms [D5]. *Commun. ACM* **1970**, *13*, 47–49. [\[CrossRef\]](#)
23. Wattenbarger, R.A.; El-Banbi, A.H.; Villegas, M.E.; Maggard, J.B. Production Analysis of Linear Flow Into Fractured Tight Gas Wells. In Proceedings of the SPE Rocky Mountain Regional/Low-Permeability Reservoirs Symposium, Denver, CO, USA, 5–8 April 1998.
24. Ezulike, D.O.; Dehghanpour, H. A model for simultaneous matrix depletion into natural and hydraulic fracture networks. *J. Nat. Gas Sci. Eng.* **2014**, *16*, 57–69.
25. Kabir, C.S.; Rasdi, F.; Igboalisi, B. Analyzing production data from tight oil wells. *J. Can. Petrol. Technol.* **2011**, *50*, 48–58. [\[CrossRef\]](#)
26. Wang, B.; Sharma, J.; Chen, J.; Persaud, P. Ensemble machine learning assisted reservoir characterization using field production data—An offshore field case study. *Energies* **2021**, *14*, 1052. [\[CrossRef\]](#)

Disclaimer/Publisher’s Note: The statements, opinions and data contained in all publications are solely those of the individual author(s) and contributor(s) and not of MDPI and/or the editor(s). MDPI and/or the editor(s) disclaim responsibility for any injury to people or property resulting from any ideas, methods, instructions or products referred to in the content.